MDPI

Article

A Reduced-Order Model of Lithium–Sulfur Battery Discharge

Noushin Haddad and Hosam K. Fathy *

Mechanical Engineering Department, The University of Maryland, College Park, MD 20742, USA; nhaddad2@umd.edu
* Correspondence: hfathy@umd.edu

Abstract: This paper examines the problem of modeling lithium–sulfur (Li-S) battery discharge dynamics. The importance of this problem stems from the attractive specific energy levels achievable by Li-S batteries, which can be particularly appealing for applications such as aviation electrification. Previous research presents different Li-S battery models, including "zero-dimensional" models that neglect diffusion while using the laws of electrochemistry to represent reduction–oxidation (redox) rates. Zero-dimensional models typically succeed in capturing key features of Li-S battery discharge, including the high plateau, low plateau, and dip point visible in the discharge curves of certain Li-S battery chemistries. However, these models' use of one state variable to represent the mass of each active species tends to furnish high-order models, with many state variables. This increases the computational complexity of model-based estimation and optimal control. The main contribution of this paper is to develop low-order state-space model of Li-S battery discharge. Specifically, the paper starts with a seventh-order zero-dimensional model of Li-S discharge dynamics, analyzes its discharge behavior, constructs phenomenological second- and third-order models capable of replicating this behavior, and parameterizes these models. The proposed models succeed in capturing battery discharge behavior accurately over a wide range of discharge rates. To the best of our knowledge, these are two of the simplest published models capable of doing so.

Keywords: lithium–sulfur batteries; data-driven modeling; discharge dynamics

1. Introduction

This paper examines the problem of building simple, reduced-order models of lithium–sulfur (Li-S) battery discharge dynamics. A typical Li-S battery cell uses a pure lithium metal sheet or chip as a negative electrode, plus a sulfur–carbon composite material as a positive electrode. Ions travel between these two electrodes through an electrolyte that can be either solid or liquid [1,2]. Significant differences exist between the dynamics of solid- versus liquid-electrolyte Li-S batteries. The focus of this paper is on modeling the dynamics of liquid-electrolyte Li-S batteries.

Liquid-electrolyte Li-S batteries are very appealing for a number of different reasons. First, they are capable of achieving much higher specific energies (i.e., energy storage capacities per unit mass) than today's commercial lithium-ion batteries [3,4]. Second, the relative abundance of sulfur as a raw material, particularly compared to rare earth metals such as cobalt, is potentially very appealing from both an environmental and economic cost perspective [5]. Finally, the use of liquid electrolytes provides a reasonable balance between the ability to deliver high levels of power versus the ability to store significant amounts of energy. This is particularly important in light of the scientific community's efforts to address the limitations of liquid-electrolyte Li-S batteries, especially those limitations created by

polysulfide shuttle [6]. Altogether, these advantages make liquid-electrolyte Li-S batteries quite appealing for emerging applications such as aviation electrification.

There is a growing literature on the modeling, estimation, and control of liquid-electrolyte Li-S battery dynamics [7–14]. Different Li-S battery models exist in the literature, spanning different levels of model fidelity versus complexity. At the more complex extreme, the literature presents models that capture the physics of both the diffusion of multiple active species and the reactions between these species. At the simpler extreme, the literature presents "zero-dimensional" Li-S battery models. These models neglect the diffusion of ions in space (hence, the term "zero-dimensional"). However, they do utilize the laws of electrochemistry to describe the rates of reduction–oxidation (redox) reactions between different active species [15–17]. Moreover, it is possible within the context of a zero-dimensional model to account for the underlying physics of species solubility and precipitation, both of which play an important role in overall battery behavior. The zero-dimensional approach typically furnishes dynamic models capable of capturing the key features of battery charge and discharge. Modeling Li-S discharge behavior is particularly important because of the complexity of this behavior as well as its impact on available discharge power and energy.

Figure 1 presents experimental discharge results for a laboratory-fabricated Li-S battery cell. The vertical axis in this figure shows the measured cell voltage, whereas the horizontal axis shows discharge capacity, normalized with respect to the maximum discharge capacity achieved in the cycling experiment. The cell was fabricated using the recipe employed in an earlier work by the authors [16]. Moreover, the above discharge curve represents relatively slow discharge, at a rate of C/9. The importance of this plot stems from the degree to which it illustrates the typical phases seen during the discharge of certain liquid-electrolyte Li-S cells. In particular, three distinct regions are visible in the plot: a high-voltage plateau, a low plateau, and a "dip point" separating these two plateaus [18,19]. The existence of these regions can be explained in terms of the multiplicity of active species involved in battery charge/discharge behavior. In a fully charged cell, the two active species are pure lithium in the negative electrode and sulfur in the positive electrode. As the battery is discharged, lithium and sulfur react to form a sequence of active species—namely Li_2S_{8aq}, Li_2S_{6aq}, Li_2S_{4aq}, and Li_2S_{aq}—and precipitated Li_2S. The transition from the high plateau to the low plateau involves the onset of the final reaction in a sequence of redox reactions involving these species. This final reaction is a precipitation reaction, and is governed by nucleation-growth dynamics [20,21]. A significant drop in voltage is required to trigger the nucleation phase of this reaction, hence the existence of the "dip point". Once nucleation occurs, battery voltage rebounds as growth takes place, which brings about the low plateau region. It is important to note that the above discharge behavior, particularly the existence of the dip point (as well as its severity), depends on the specific battery chemistry under examination, including the choice of electrolyte. Dip point behavior is especially visible for the high-solubility DME/DOL electrolyte combination employed in the fabrication of the battery cell used in Figure 1.

The literature presents a number of different models capable of capturing the above Li-S battery discharge behavior accurately. Regardless of the type of model, one common challenge is that practically all Li-S battery models in the literature suffer from significant computational complexity. At least three reasons exist for this complexity:

- First, as explained above, the process of charging and discharging Li-S batteries involves a sequence of reduction–oxidation reactions. Multiple chemical species are involved in these reactions. This creates a need for higher-order models, where the concentration of each chemical species is represented by a state variable. This can be

particularly problematic for optimal control applications, given Bellman's curse of dimensionality [22].

- Second, the dynamics of Li-S batteries are highly nonlinear. One cause of this nonlinearity is the nucleation-growth process responsible for precipitation reactions in these batteries. The dynamics of this nucleation-growth process play a very visible role in overall battery discharge behavior, especially the existence of the above "dip point". This makes it important to model the nonlinearities of these batteries, and therefore difficult to approximate their dynamics as linear.

- Third, the rates of different reactions in Li-S batteries are highly dependent on species concentrations, in a manner that leads to numerical model stiffness.
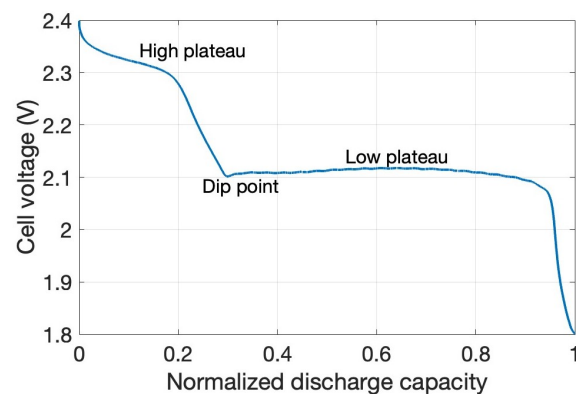
Figure 1. Li-S battery discharge voltage characteristics.

Previous research in the literature attempts to address the above challenges through model reduction and simplification [16,23]. However, even the simplest models of liquid-electrolyte Li-S battery dynamics in the literature remain relatively complex compared to simple lithium-ion battery models. The main contribution of this work is to show that it is possible to build a low-order Li-S battery model that captures constant-current discharge dynamics accurately, over a broad range of discharge currents. Towards this goal, the paper begins by exploring a baseline seventh-order Li-S battery model from the literature (Section 2). Simulating this model provides insights into the underlying behavior of the battery's state variables during discharge (Section 3). These insights motivate the paper's own model (Section 4). The model is constructed in a "phenomenological" manner, meaning that its mathematical structure is designed to replicate the dynamic behaviors seen in the higher-order baseline model from the literature. The paper fits this reduced-order model to the simulation results from the higher-order baseline model (Section 5). The quality of fit is quite appealing, across a broad range of discharge rates. The end result is a model that captures the discharge dynamics of liquid-electrolyte Li-S batteries accurately, over a broad range of constant discharge rates, while only containing two to three state variables. In particular, a second-order version of this model achieves excellent simulation accuracy for low C-rates, and reasonable accuracy at higher C-rates. Moreover, a third-order version of this model achieves excellent simulation accuracy across a very wide range of C-rates. To the best of the authors' knowledge, these two variants of the proposed model are some of the lowest-order models in the literature capable of simulating Li-S battery discharge accurately. The primary limitation of such data-driven, or "phenomenological", reduced-order modeling is the fact that phenomenological models need to be re-fitted for different battery chemistries. Physics-based models, in contrast, are more easily transferable from one chemistry to another because of the generalizability of the underlying fundamental laws of electrochemistry, but this often comes at the expense of high computational complexity.

2. Baseline Model

This section presents a baseline zero-dimensional model of Li-S battery discharge. This model was originally developed by the electrochemistry community [15]. More recent research by the authors and colleagues examined the parameterization of this model from experimental data, as well as the simplification of this model for control applications [16]. The model contains seven state variables. Five of these state variables represent the masses of active species involved in Li-S battery redox reactions. The sixth state variable represents the mass of the final precipitated species, and the seventh state variable represents the porosity of the positive electrode material, which is influenced by precipitation. The dynamics of the resulting seven state variables can be summarized using the equations below.

First, let the masses of the various dissolved species in the Li-S battery be represented by m_i, where $i = 1, \ldots, q$ is the index of a given species and q is the total number of soluble active species. Furthermore, let j be an index used for distinguishing between various redox reactions in the Li-S battery, and let i_j denote the effective current associated with redox reaction j. Then, the law of conservation of mass can be used for expressing the rates of change of all the dissolved active species not involved in the precipitation reaction, as shown below (where all remaining terms in the equation are constant parameters):

$$\dot{m}_i = \sum_j \frac{n_{S_i} M_s}{n_j F} s_{i,j} i_j \, , \quad \text{for } i = 1, \ldots, q-1 \tag{1}$$

Next, the rate of change of the mass of the active species involved in the precipitation reaction, as well as the rate of change of the mass of the precipitate, m_{S_p}, are governed by

$$\dot{m}_q = \frac{n_{S_q} M_s}{n_p F} s_{q,p} i_p - \dot{m}_{S_p} \tag{2}$$

$$\dot{m}_{S_p} = k_p m_{S_p} (m_q - S_{sat}) \tag{3}$$

where S_{sat} is a saturation value of dissolved species mass, and all other terms in the above state equations are constant. The use of the saturation value, S_{sat}, in this model, essentially accounts for maximum species solubility.

Next, the rate of change of solid electrode porosity is related to the rate of precipitation as follows:

$$\dot{\varepsilon} = -\omega \dot{m}_{S_p} \tag{4}$$

Next, the effective reaction currents appearing in the above state equations are governed by the Butler–Volmer equation, a fundamental law of electrochemistry:

$$i_j = -a_v i_j^0 \left\{ \prod_i \left(\frac{m_i}{m_i^0} \right)^{s_{i,j}} e^{\frac{F}{2RT} \eta_j} - \prod_i \left(\frac{m_i}{m_i^0} \right)^{-s_{i,j}} e^{-\frac{F}{2RT} \eta_j} \right\} \tag{5}$$

where the rate of each reaction is related to porosity through the following equation for the active reaction area:

$$a_v = a_v^0 \varepsilon^\gamma \tag{6}$$

Next, the overpotentials driving the above Butler–Volmer equation can be expressed in terms of the terminal battery voltage, V, and the reference potential for each reaction, E_j, as follows:

$$V = \eta_j + E_j \tag{7}$$

Next, the above reference potentials are related to species masses through the Nernst equation, another fundamental law of electrochemistry:

$$E_j = E_j^0 - \frac{RT}{n_j F} \sum_i s_{i,j} \ln\left(\frac{m_i}{n_{S_i} M_s v}\right) \tag{8}$$

Finally, the total battery current can be expressed as the sum of the individual reaction currents as follows:

$$I = \sum_j i_j \tag{9}$$

Altogether, the above equations form a differential algebraic equation (DAE) model that can be used for simulating Li-S battery discharge behavior. More details of this model's equations and parameters can be found in the authors' previous publications and earlier work from the electrochemistry literature [15,16]. The use of this model for optimal control studies is challenging because of its order, nonlinearity, numerical stiffness, and the fact that, as a DAE model, it contains an algebraic loop as opposed to consisting solely of explicit state equations.

3. Baseline Simulation

Figure 2 shows the results of simulating the above physics-based Li-S battery model for a discharge rate of 1 C, assuming a 3 Ampere-hour cell. The horizontal axis represents normalized discharge capacity, whereas the vertical axis represents the values of the model's state variables. Six of the state variables represent the masses of either an active or precipitated species, whereas the seventh state variable represents porosity. This simulation is performed for the DAE model in section 2, reproducing earlier research by the investigators [16].
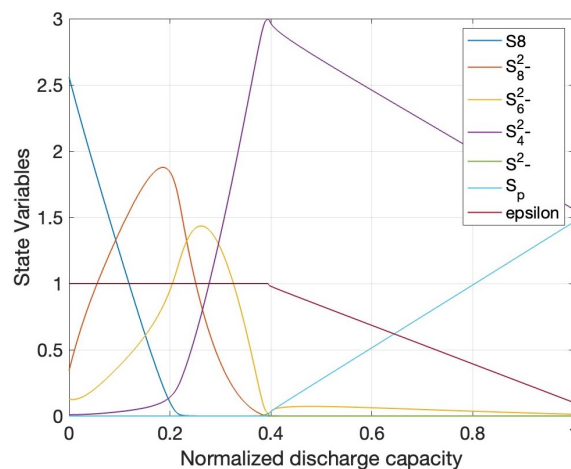

Figure 2. Species mass histories for 1 C discharge.

The results in Figure 2 are particularly effective in explaining some of the complexities associated with Li-S battery discharge modeling. As the figure clearly shows, battery discharge involves a sequence of redox reaction, with each reaction causing a rise in the concentration of a given active species before the next reaction depletes that concentration. The transition between the high and low plateaus coincides with the onset of a precipitation reaction that consumes a single active species, producing a precipitate that also influences porosity.

The discharge voltage profile corresponding to Figure 2 is shown in Figure 3. The fact that this voltage profile shows a high plateau, low plateau, and dip point is consistent with the degree to which zero-dimensional models are capable of capturing typical Li-S battery discharge characteristics. The severity of dip point behavior depends at least partially on the C-rate. Given the fact that this model is being simulated for a relatively large C-rate of 1 C, it is not surprising to see significant dip behavior. The model is only simulated until a low plateau voltage of approximately 1.95 V is reached. During laboratory cycling,

liquid-electrolyte Li-S cells are often discharged down to voltage levels at the order of 1.7–1.8 V. However, as seen in Figure 1, once cell voltage drops to the 1.9–2 V range, the remaining battery discharge capacity is typically very small. Therefore, the above DAE model was designed in previous research to capture discharge characteristics down to a voltage of roughly 1.9–2 V.

The goal of this paper is not to build a physics-based model capable of predicting the above histories of the various active species masses. Rather, we seek a much simpler model that can accurately capture the corresponding discharge voltage behavior, shown in Figure 3. Ideally, such a model should consist of a small number of explicit ordinary differential equations, and should be accurate over a broad range of discharge C-rates. This is a challenging problem, given the degree to which Li-S battery discharge dynamics change in nature with C-rate. Figures 4 and 5 illustrate this degree by showing different discharge voltage curves, simulated for C-rates ranging from 0.02 C to 1 C. The plot in Figure 4 shows time on the x-axis without scaling, whereas the plot in Figure 5 uses normalized discharge capacity as its independent variable. The intent in showing the same results twice versus time and discharge capacity is to emphasize the fact that Li-S battery discharge behavior is strongly dependent on C-rate. Discharge time/rate is important when examining Li-S battery discharge; it fundamentally affects the shape of the discharge characteristics curve. For example, the severity of the dip point and the final battery discharge voltage both show very strong variations with the C-rate. This adds complexity to the paper's model reduction goal. Section 4 proposes a model that addresses this complexity successfully.
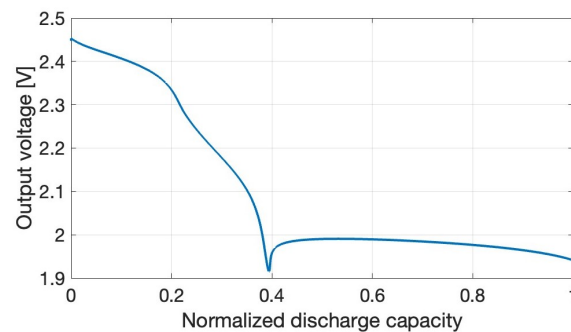

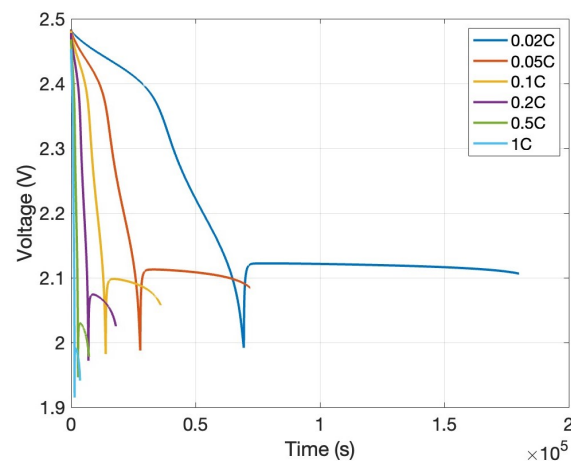**Figure 3.** Simulated discharge at a 1 C rate.

Figure 4. Li-S discharge voltage characteristics for different C-rates.
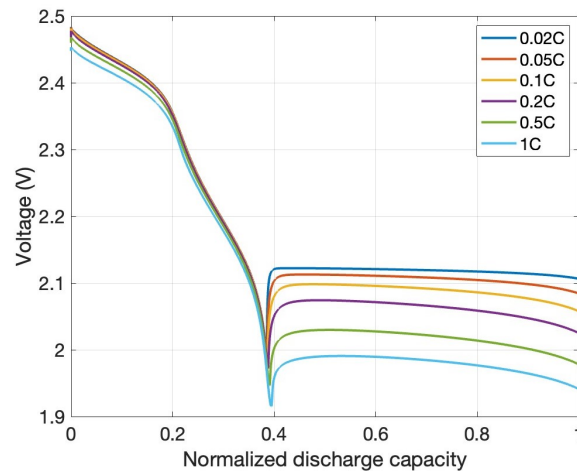
Figure 5. Discharge characteristics versus scaled discharge capacity.

4. Proposed Model

The key idea behind the proposed model is to embrace a "phenomenological" modeling approach, where different elements of the model reflect different battery discharge behaviors. Three state variables are employed by the model to capture four specific behaviors. The first state variable, $x_1(t)$, captures *(i)* a relationship between open-circuit voltage and state of charge for extremely slow discharge, with the dip point and the recovery from this dip point both deliberately removed from the discharge characteristics. The second state variable, $x_2(t)$, captures the dynamics of traversing the dip point. This includes the dynamics associated with *(ii)* "dipping", as well as the dynamics associated with *(iii)* "recovery" from the dip point. Finally, the third state variable, $x_3(t)$, captures the dynamics of *(iv)* voltage decay in the low plateau. Figure 5 shows that these dynamics are more prominent at higher C-rates. This means that the state equation for $x_3(t)$ is more valuable for modeling higher C-rate behavior. Given these choices of state variables, the proposed model has the following structure:

$$\dot{x}_1 = \frac{-u}{Q} \tag{10}$$

$$\dot{x}_2 = I_1(x_1)\lambda_1 x_2 + I_2(x_1)\lambda_2(x_2^* - x_2) \tag{11}$$

$$\dot{x}_3 = I_2(x_1)\lambda_3 x_3 \tag{12}$$

$$y = g(x_1) - x_2 - x_3 - R_s u \tag{13}$$

where $u(t)$ is discharge current, $y(t)$ is discharge voltage, R_s is an effective Ohmic series resistance, $\lambda_{1,2,3}$ are the magnitudes of eigenvalues associated with different battery dynamics, Q is battery charge capacity, and $I_{1,2}(x_1)$ are indicator functions that equal unity during dipping and recovery, respectively. In particular, these indicator functions are given by

$$I_1(x_1) = \mathcal{U}(x_1 - x_d)(1 - \mathcal{U}(x_1 - x_r))$$
$$I_2(x_1) = \mathcal{U}(x_1 - x_r) \tag{14}$$

where $\mathcal{U}$ is the unit step function, x_d is the state of charge associated with the onset of dipping, and x_r is the state of charge associated with the onset of recovery.

The structure of the above model is tailored in a manner that recognizes the fundamental change in battery behavior associated with the traversal of the dip point and recovery from it. In particular, the model uses the function $g(x_1)$ to represent a low C-rate open-circuit potential that depends solely on state of charge. Corrections are made to this open-circuit potential through the dynamics of $x_2(t)$: a state variable that experiences rapid

(in fact, dynamically unstable) growth at an eigenvalue λ_1 during dipping, but recovers to some value x_2^* in a manner governed by an eigenvalue $-\lambda_2$ after dipping. Finally, an additional correction is made during recovery from dipping by allowing an optional third state variable, $x_3(t)$, to grow at an exponential rate governed by an eigenvalue λ_3 in the low plateau region. This third state variable is, therefore, intended to capture the curvature of the voltage profile versus time in the low plateau region.

Intuitively, one expects the parameters of the above model to depend on discharge C-rate. To appreciate this, examine the discharge voltage curves in Figures 4 and 5. Higher C-rates translate to sharper dip points when the time axis is not scaled, meaning that the "dipping" behavior occurs faster. Recovery from dipping at higher C-rates also occurs faster, but to lower values of final voltage after recovery. Moreover, the curvature of the low plateau region is more pronounced for higher C-rates, especially when examined versus normalized/scaled discharge capacity. Altogether, these observations suggest that the parameters of the proposed model need to be fitted differently for each C-rate. Cohesiveness can still be achieved among different models associated with different C-rates by forcing the function $g(x_1)$ to be the same regardless of C-rate. This motivates the model fitting approach in Section V.

5. Model Fitting

To fit the above model to Li-S battery discharge behavior at multiple C-rates, we begin by simulating discharge at a very low rate of 0.02 C. Then, we tailor the function $g(x_1)$ such that it meets two criteria. First, the function $g(x_1)$ equals the discharge voltage at 0.02 C at every state of charge outside a user-selected window that surrounds the dip point. Second, inside the above user-selected window, the function $g(x_1)$ is a cubic function that merges with the discharge voltage profile at the boundaries of the window with C^1 continuity. In other words, the values and slopes of the function $g(x_1)$ match the discharge voltage profile at the edges of the above user-selected window.

Figure 6 shows the results of the above initial fitting exercise. The red curve represents the function $g(x_1)$, which in turn represents open-circuit voltage (OCV) versus state of charge (SOC). The blue curve, in contrast, represents discharge voltage versus state of charge for a 0.02C discharge. Intuitively, the idea behind the above figure is to define an OCV-SOC curve that reflects the traditional approach for measuring OCV versus SOC in the laboratory, namely, the use of very slow cycling for such measurement. However, the fitting process also accounts for the existence of the dip point, and for the fact that voltage dipping behavior in Li-S cells is governed by transient dynamics, as opposed to steady-state characteristics. Such transient dynamics exist even at very low C-rates, prompting the above approach for extracting a representative OCV-SOC curve. One should note that this curve is only an approximation of OCV-SOC behavior at infinitely slow discharge. Moreover, one should note that the nonlinear nature of Li-S battery dynamics creates the possibility that multiple OCV-SOC curves may exist for a given battery. The goal, in this fitting exercise, is to use a "representative" slow discharge curve to construct the function $g(x_1)$. This function is then used as a foundation for fitting other elements of the proposed Li-S battery model, as discussed below. Forcing the function $g(x_1)$ to be the same for all discharge rates ensures some degree of consistency and commonality among the different battery models fitted for different C-rates.

Given the above OCV-SOC curve, we fitted the remaining elements of the proposed model to the baseline higher-order Li-S battery model as follows. First, we selected a representative set of six C-rates, namely, 0.02 C, 0.05 C, 0.1 C, 0.2 C, 0.5 C, and 1 C. Next, for each C-rate, we simulated the baseline model to obtain discharge voltage versus time. Next, keeping the function $g(x_1)$ fixed, we optimized a vector of eight model parameters

independently for each C-rate. This vector included the following: *(i,ii)* the initial conditions for $x_2(t)$ and $x_3(t)$ at the beginning of discharge; *(iii,iv)* the parameters x_d and x_r governing the onset of dipping and recovery, respectively; *(v)* the parameter x_2^* affecting the voltage at the end of recovery; and *(vi,vii,viii)* the parameters $\lambda_{1,2,3}$ governing the rates of dipping/recovery as well as the curvature of the low plateau. The optimization objective was to minimize the sum of the squared differences between the discharge voltage profiles associated with the baseline model versus the proposed model.
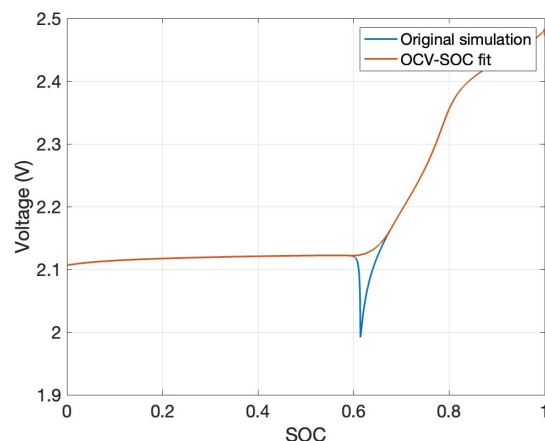

Figure 6. Results of fitting open-circuit voltage versus state of charge.

Figures 7 and 8 provide two snapshots of the optimization results associated with the most extreme C-rates examined, namely, 1 C and 0.02 C. Both plots show discharge voltage behavior versus time in order to emphasize the fact that the two plots correspond to drastically different C-rates, and therefore significantly different discharge characteristics. The quality of fit is excellent across the board, for all C-rates examined. Table 1 emphasizes this conclusion by listing the root mean square (RMS) voltage deviations of the reduced-order model from the benchmark model for each C-rate. Moreover, Table 2 lists the model parameter values associated with this fitting.

Table 1. Accuracy of third-order model.

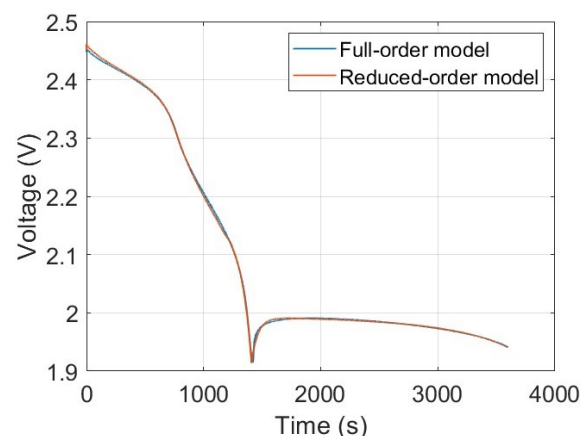| C-rate	0.02	0.05	0.1	0.2	0.5	1
RMSE (mV)	1.57	1.27	2.55	1.54	2.00	3.33

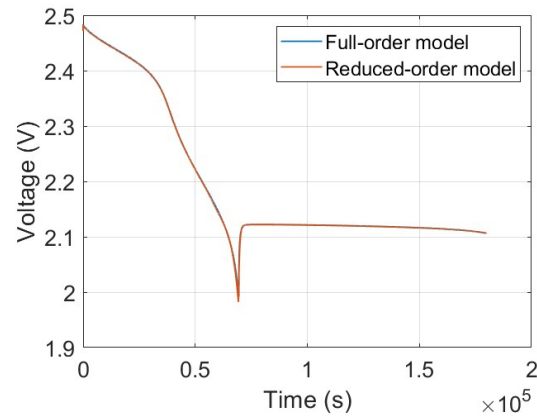**Figure 7.** Discharge voltage at 1 C-rate.

Figure 8. Discharge voltage at 0.02 C-rate.

The accuracy of the above fitting results is a direct consequence of the fact that there are three state variables in the proposed model, with the third state variable representing the curvature of the low plateau. This curvature matters most for higher C-rates, given the higher-order dynamics excited by these C-rates. This presents an intriguing possibility of fitting a second-order model, where the dynamics of $x_3(t)$ are neglected. Table 3 lists the RMS voltage prediction errors obtained when a second-order version of the proposed model is fitted to the results of the full-order model. Excellent accuracy levels are obtained for low C-rates. However, significant deterioration in accuracy is visible at higher C-rates, corresponding to the reduced ability of the model to capture the curvature of the high plateau. Overall, the model continues to be reasonably accurate across all C-rates—a very encouraging result given the fact that this is a second-order model. However, it is worth noting that capturing battery dynamics accurately at higher C-rates requires a higher-order model. This finding makes intuitive sense, considering the fact that higher C-rates do trigger higher-order dynamics in electrochemical batteries. Figures 9 and 10 reinforce this insight by showing the fitting results at both a low C-rate (namely, 0.02 C) and a high C-rate (namely, 1 C). The second-order model clearly fits the lower C-rate better, with the deterioration at the higher C-rate visually appearing in the form of poor capturing of the curvature of the low plateau.

Table 2. Third -order model parameters.

C-rate	0.02	0.05	0.1	0.2	0.5	1
$x_2(0)$ (mV)	0.62	1.29	0.1	3.29	8.00	2.75
$x_3(0)$ (mV)	0.102	0.107	0.644	1.049	1.248	0.869
x_d	0.70	0.69	0.72	0.68	0.67	0.68
x_r	0.62	0.61	0.62	0.61	0.61	0.60
$1000\lambda_1$	0.36	0.84	2.06	3.18	7.26	16.53
$1000\lambda_2$	2.00	2.93	3.52	5.91	11.90	18.38
$1000\lambda_3$	0.002	0.108	0.166	0.318	0.780	1.70
x_2^* (mV)	0.10	9.77	21.87	46.83	88.63	111.6
R_s (mΩ)	0.008	0.005	4.74	0.001	1.17	6.01

Table 3. Accuracy of second-order model.

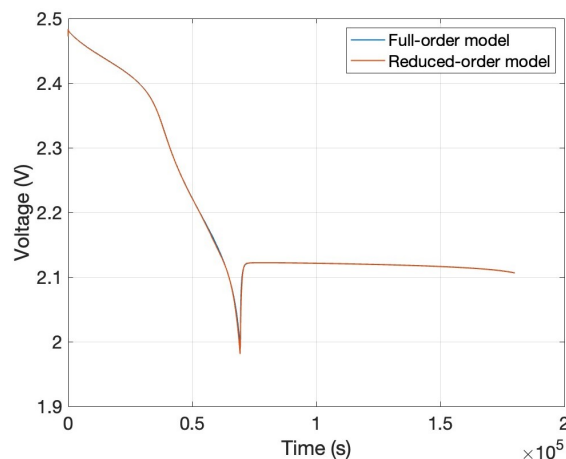| C-rate	0.02	0.05	0.1	0.2	0.5	1
RMSE (mV)	1.45	2.75	5.14	6.97	7.61	7.37

Figure 9. Second-order model fitting results at 0.02 C.
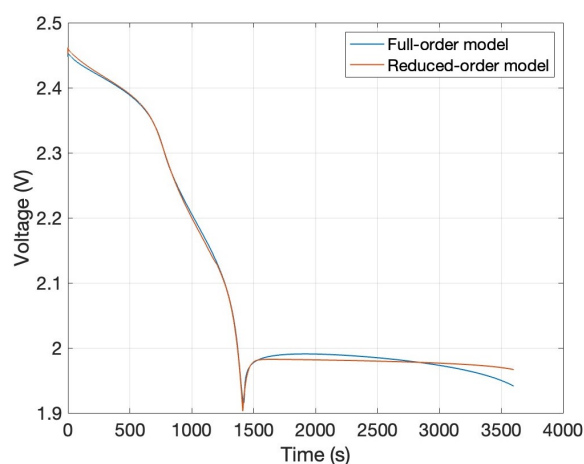

Figure 10. Second-order model fitting results at 1 C.

6. Conclusions

The main contribution of this paper is to show that a pair of simple and intuitive low-order models are capable of capturing the discharge behavior of a liquid-electrolyte Li-S battery accurately over a broad range of C-rates. These models can be quite valuable for battery estimation and control studies, given their low order. One particularly important feature of these models is the fact that they enforce uniformity and consistency across different C-rates by ensuring the adoption of a single representative OCV-SOC curve across all these C-rates. A tradeoff exists between the computational simplicity of the reduced-order models presented in this paper versus the inherent difficulty associated with applying them to different battery chemistries. Specifically, because these models are "phenomenological", as opposed to physics-based, they may require re-fitting to different Li-S battery chemistries. This makes it potentially harder to generalize the models to multiple chemistries in comparison to physics-based modeling approaches—a sacrifice that may be quite reasonable considering the associated significant reduction in model complexity.

Author Contributions: Conceptualization, H.K.F. and N.H.; methodology, H.K.F.; software, N.H. and H.K.F.; validation, N.H.; formal analysis, N.H. and H.K.F. investigation, N.H. and H.K.F.; resources, H.K.F.; data curation, N.H.; writing—original draft preparation, N.H. and H.K.F.; writing—review and editing, H.K.F. and N.H.; visualization, N.H.; supervision, H.K.F.; project administration, H.K.F.; funding acquisition, H.K.F. All authors have read and agreed to the published version of the manuscript.

Batteries **2025**, *11*, 15

12 of 13

Funding: This research was funded by the United States Naval Air Warfare Center Aircraft Division (NAW-CAD) Grant Number "1301117611".

Data Availability Statement: Dataset available on request from the authors.

Acknowledgments: Support for this research was provided by the United States Naval Air Warfare Center Aircraft Division (NAWCAD). The authors gratefully acknowledge this support (NAWCAD distribution statement: approved for public release; distribution is unlimited). The opinions in this paper are those of the authors, and do not necessarily reflect the opinions of the research sponsor.

Conflicts of Interest: The authors declare no conflicts of interest.

References

1. Wild, M.; O'neill, L.; Zhang, T.; Purkayastha, R.; Minton, G.; Marinescu, M.; Offer, G. Lithium sulfur batteries, a mechanistic review. *Energy Environ. Sci.* **2015**, *8*, 3477–3494. [CrossRef]
2. Shi, C.; Takeuchi, S.; Alexander, G.V.; Hamann, T.; O'Neill, J.; Dura, J.A.; Wachsman, E.D. High sulfur loading and capacity retention in bilayer garnet sulfurized-polyacrylonitrile/lithium-metal batteries with gel polymer electrolytes. *Adv. Energy Mater.* **2023**, *13*, 2301656. [CrossRef]
3. Bresser, D.; Passerini, S.; Scrosati, B. Recent progress and remaining challenges in sulfur-based lithium secondary batteries-a review. *Chem. Commun.* **2013**, *49*, 10545–10562. [CrossRef]
4. Bruce, P.G.; Freunberger, S.A.; Hardwick, L.J.; Tarascon, J.-M. Li-O$_2$ and Li-S batteries with high energy storage. *Nat. Mater.* **2012**, *11*, 19–29. [CrossRef] [PubMed]
5. Dehghani-Sanij, A.; Tharumalingam, E.; Dusseault, M.; Fraser, R. Study of energy storage systems and environmental challenges of batteries. *Renew. Sustain. Energy Rev.* **2019**, *104*, 192–208. [CrossRef]
6. Gu, S.; Sun, C.; Xu, D.; Lu, Y.; Jin, J.; Wen, Z. Recent progress in liquid electrolyte-based Li-S batteries: Shuttle problem and solutions. *Electrochem. Energy Rev.* **2018**, *1*, 599–624. [CrossRef]
7. Parke, C.D.; Teo, L.; Schwartz, D.T.; Subramanian, V.R. Progress on continuum modeling of lithium–sulfur batteries. *Sustain. Energy Fuels* **2021**, *5*, 5946–5966. [CrossRef]
8. Fotouhi, A.; Auger, D.J.; Propp, K.; Longo, S.; Purkayastha, R.; O'Neill, L.; Waluś, S. Lithium–sulfur cell equivalent circuit network model parameterization and sensitivity analysis. *IEEE Trans. Veh. Technol.* **2017**, *66*, 7711–7721. [CrossRef]
9. Jiang, J.; Liang, Y.; Ju, Q.; Zhang, L.; Zhang, W.; Zhang, C. An equivalent circuit model for lithium-sulfur batteries. *Energy Procedia* **2017**, *105*, 3533–3538. [CrossRef]
10. Knap, V.; Stroe, D.-I.; Teodorescu, R.; Swierczynski, M.; Stanciu, T. Electrical circuit models for performance modeling of lithium-sulfur batteries. In Proceedings of the 2015 IEEE Energy Conversion Congress and Exposition (ECCE), Montreal, QC, Canada, 20–24 September 2015; pp. 1375–1381.
11. Kumaresan, K.; Mikhaylik, Y.; White, R.E. A mathematical model for a lithium–sulfur cell. *J. Electrochem. Soc.* **2008**, *155*, A576. [CrossRef]
12. Propp, K.; Marinescu, M.; Auger, D.J.; O'Neill, L.; Fotouhi, A.; Somasundaram, K.; Offer, G.J.; Minton, G.; Longo, S.; Wild, M.; et al. Multi-temperature state-dependent equivalent circuit discharge model for lithium-sulfur batteries. *J. Power Sources* **2016**, *328*, 289–299. [CrossRef]
13. Ren, Y.; Zhao, T.; Liu, M.; Tan, P.; Zeng, Y. Modeling of lithium-sulfur batteries incorporating the effect of Li$_2$S precipitation. *J. Power Sources* **2016**, *336*, 115–125. [CrossRef]
14. Zhang, T.; Marinescu, M.; O'Neill, L.; Wild, M.; Offer, G. Modeling the voltage loss mechanisms in lithium–sulfur cells: The importance of electrolyte resistance and precipitation kinetics. *Phys. Chem. Chem. Phys.* **2015**, *17*, 22581–22586. [CrossRef] [PubMed]
15. Marinescu, M.; Zhang, T.; Offer, G.J. A zero dimensional model of lithium–sulfur batteries during charge and discharge. *Phys. Chem. Chem. Phys.* **2016**, *18*, 584–593. [CrossRef]
16. Xu, C.; Cleary, T.; Li, G.; Wang, D.; Fathy, H. Parameter identification and sensitivity analysis for zero-dimensional physics-based lithium-sulfur battery models. *ASME Lett. Dyn. Syst. Control* **2021**, *1*, 041001. [CrossRef]
17. Huang, Z.; Zhang, D.; Couto, L.D.; Yang, Q.-H.; Moura, S.J. State estimation for a zero-dimensional electrochemical model of lithium-sulfur batteries. In Proceedings of the 2021 American Control Conference (ACC), New Orleans, LA, USA, 25–28 May 2021; pp. 3114–3119.
18. Nozarijouybari, Z.; Fang, C.; Doosthosseini, M.; Xu, C.; Fathy, H.K. An algorithm for dip point detection in lithium–sulfur battery cells. *J. Energy Storage* **2022**, *55*, 105665. [CrossRef]
19. Ning, G.; Popov, B.N. Cycle life modeling of lithium-ion batteries. *J. Electrochem. Soc.* **2004**, *151*, A1584. [CrossRef]

20. Andrei, P.; Shen, C.; Zheng, J.P. Theoretical and experimental analysis of precipitation and solubility effects in lithium-sulfur batteries. *Electrochim. Acta* **2018**, *284*, 469–484. [CrossRef]

21. Danner, T.; Latz, A. On the influence of nucleation and growth of S_8 and Li_2S in lithium-sulfur batteries. *Electrochim. Acta* **2019**, *322*, 134719. [CrossRef]

22. Bellman, R. Dynamic programming. *Science* **1966**, *153*, 34–37. [CrossRef] [PubMed]

23. Knap, V.; Stroe, D.-I.; Teodorescu, R.; Swierczynski, M.; Stanciu, T. Comparison of parametrization techniques for an electrical circuit model of lithium-sulfur batteries. In Proceedings of the 2015 IEEE 13th International Conference on Industrial Informatics (INDIN), Cambridge, UK, 22–24 July 2015; pp. 1278–1283.